Article

A Novel Thermal Module with 3-D Configuration Pulsating Heat Pipe for High-Flux Applications

Chih-Yung Tseng [1,3], Ho-Meng Wu [2], Shwin-Chung Wong [2], Kai-Shing Yang [1] and Chi-Chuan Wang [3,*]

[1] Green Energy & Environment Research Laboratories, Industrial Technology Research Institute, 195, Sec.4, Chung Hsing Rd., Hsinchu 31040, Taiwan; chihyungtseng@itri.org.tw (C.-Y.T.); ksyang@itri.org.tw (K.-S.Y.)

[2] Department of Power Mechanical Engineering, National Tsing Hua University, 101, Sec.2 Kuang Fu Rd., Hsinchu 30013, Taiwan; itri455034@itri.org.tw (H.-M.W.); scwong@pme.nthu.edu.tw (S.-C.W.)

[3] Department of Mechanical Engineering, National Chiao Tung University, EE474, 1001 University Rd., Hsinchu 30010, Taiwan

* Correspondence: ccwang@mail.nctu.edu.tw; Tel.: +886-3-5712121

Abstract: A pulsating heat pipe (PHP) contains a wickless design with aligned serpentine tube configuration whose simple structure offers a comparatively easy manufacturing capability. The bends with large curvature are often used for serpentine PHPs. This eventually results in a decline in effective contact surface area between evaporator/condenser and PHP circuitry, thereby impairing the benefit of the wickless design of a PHP. A novel thermal module featuring a 3-D configuration pulsating heat pipe, an evaporator, and a fin-and-tube condenser is proposed to tackle the high-flux application. Methanol is used as the working fluid with a filling ratio of around 60%. Test results indicate the thermal resistance of the proposed module varies from 0.148 K/W to 0.0595 K/W when the supplied power changes from 100 to 1000 W. The proposed thermal module can handle a supplied power up to 1 kW and the corresponding power or heat flux is much higher than any existing literatures.

Keywords: pulsating heat pipe; thermal resistance; junction temperature; thermal module

1. Introduction

In contrast to the conventional heat pipes as shown in Figure 1, the pulsating heat pipe (PHP) contains a wickless design with aligned serpentine tube configuration. The heat transportation in a conventional heat pipe is accomplished through liquid evaporation at the heat source followed by condensation at the heat sink, and finally the condensate liquid moves back to the evaporator via wick structures through the utilization of capillary force [1–3]. Unlike conventional heat pipes, the PHP is filled with more working fluid. The received heat from the evaporator then creates bubbles and increases vapor pressure that forces the fluid toward the condenser. Eventually, the bubbles collapse by heat dissipation in the condenser section, and the heat transfer mechanism is mainly by self-exciting oscillation which is also driven by a fast fluctuating pressure wave engendered from nucleate boiling and subsequent condensation of the working fluid as shown in Figure 2. PHP is wickless and simple in structure, and offers a comparatively easy manufacturing capability [4,5]. Yet it also contains many outstanding features like long distance transportation capability, a large heat dissipation surface area, flexibility in tubing design, highly effective thermal conductivity, and is applicable in high-flux applications.
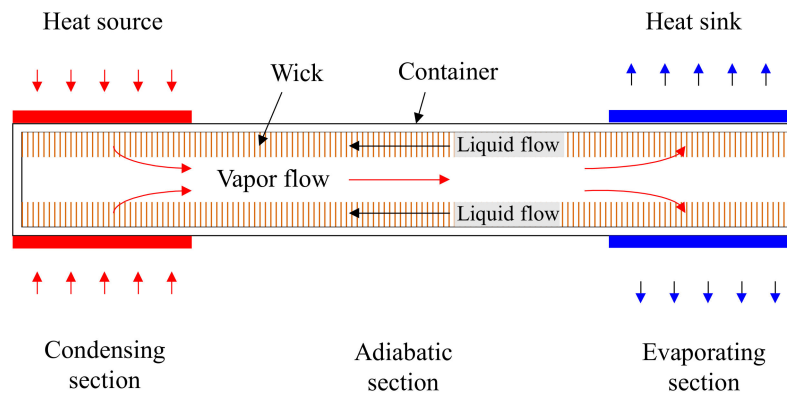
Figure 1. Schematic of a conventional heat pipe showing the principle of operation and circulation of the working fluid.
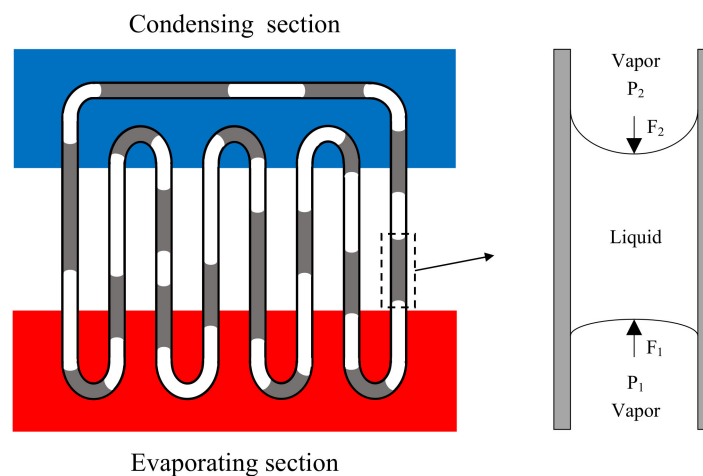

Figure 2. Basic structure of typical pulsating heat pipe (PHP).

Despite the fact that the PHP has been in existence for several decades, real products in practice are very rare in commercial cooling systems. The key problem is due to its comparable difficulty in starting up when compared to other types of heat pipe. In steady state the pressures between neighboring tubes may be in equilibrium, thereby failing to move the oscillating liquid slug to and fro effectively. Moreover, the PHP cannot be activated for fewer turn designs if the heat source is placed on top due to poor mobility of accumulated liquid at the bottom. To tackle the limitations in the starting up characteristics of PHPs subject to horizontal orientation, Chien et al. [6] proposed an alternating tube size that introduces an unbalanced capillary force. By incorporating different cross sectional areas amid adjacent tubes of the PHP, additional unbalancing force caused by pressure force and capillary force can offer a uni-directional movement of the liquid slug and successfully launch the PHPs subject to a horizontal arrangement. Yang et al. [7,8] extended this concept further in silicon-based micro PHPs by analyzing the flow patterns and heat transfer performance. Tseng et al. [9] developed some similar designs for PHPs having distilled water, methanol, and HFE-7100 as the working fluids. They found that a working fluid with a larger slope of $(dP/dT)_{sat}$ like HFE-7100 may offer a comparatively easy start-up characteristic at a low supplied heating power, thereby exhibiting a lower thermal resistance accordingly. However, water is still superior to other working fluids at a higher supplied power due to its much higher latent heat and specific heat.

Although the foregoing studies had resolved the startup of PHPs subject to horizontal arrangement, PHP is still not functional when placing the heat source/sink upside down. This apparently limits the applicability of PHP in facing real world applications (for instance, some lighting products, e.g., projectors or LED lighting may have the heat sources on top).

Hence, Tseng et al. [10] proposed a novel design of the PHP which contains connected plural number of tubes. The design introduces even more pronounced unbalanced force, and works very well even for a PHP with a few turns, and it is also applicable for inverting the heat source from bottom to top. The lowest thermal resistance subject to an inverted heat source is 0.0729 W/K, corresponding to an effective thermal conductivity of 12,603 $W \cdot m^{-1} \cdot K^{-1}$. Sun et al. [11] verify the effect of evacuation pressure on the performance and startup characteristics of a PHP using water and HFE-7000. They concluded that a PHP operated with water is appreciably influenced by evacuation pressure as compared to HFE-7000. A PHP with HFE-7000 can be activated even without any evacuation.

The existing studies aimed at improving the thermal performance of the PHP itself. One of the outstanding features for the PHP is its wickless design that relieves the capillary limit to some extent as compared to the conventional heat pipes. By imposing supplied heat onto the PHP, the liquid evaporates and expands accordingly to move the liquid slug to and fro, thereby effectively absorbing heat from evaporator and then giving up heat at the condenser. For the typical PHP as shown in Figure 2, a small diameter tube is normally employed with serpentine configuration to make use of capillary force. Yet bends formed in the condenser/evaporator sections normally require careful mechanical machining to avoid severe deformations. In this regard, bends with large curvature are often used for serpentine PHPs. Unfortunately, this eventually results in a decline in effective contact surface area between evaporator/condenser and PHP circuitry, thereby impairing the benefit of the wickless design of the PHP. In essence, although the PHP can offer high-flux transporting capability, the thermal module incorporating PHPs normally fails to meet the high-flux demand. For further clarification of this problem, observe Figure 3 which demonstrates the thermal resistance distribution in a typical PHP by Sun et al. [11]. Using water as the working fluid, the largest resistance is from the evaporator to the PHP ($R_{evap\text{-}BE}$, 45.51%) and PHP to condenser ($R_{BC\text{-}cond}$, 31.58%). Note that Sun et al. [11] adopted a water-cooled condenser whose performance is much superior to an air-cooled condenser. Hence, the thermal resistance for an air-cooled design should easily surpass 31.58% for an air-cooled design. In summary, the design of the evaporator and condenser is even more important as far as overall performance of a thermal module is concerned.
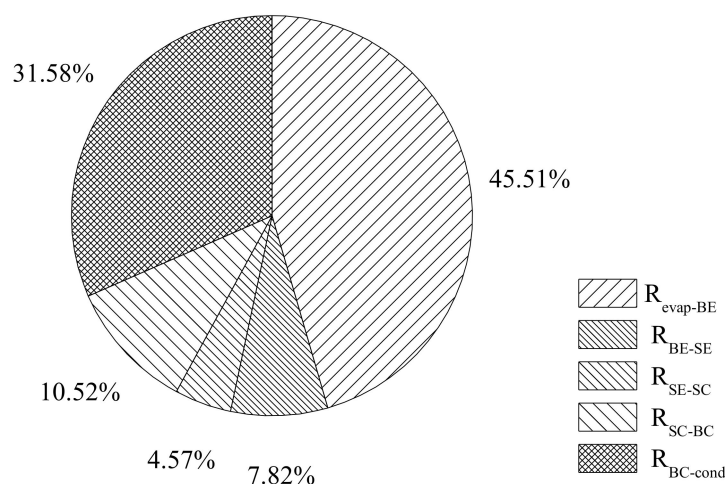

Figure 3. Thermal resistance distribution (%) for traditional PHP thermal module. The original raw data is taken from [11], and replots using a different kind of schematic for presentation.

Prior research had resolved some technical difficulties of PHPs, and most of the existing studies for PHPs focused on the performance of PHPs subject to some operational parametric effects, such as the influence of various working fluids [9], filling ratios [12], and tilt angle [13]. However, very rare studies had incorporated the PHPs into thermal modules to tailor the high-flux applications. In this regard, it is the objective of this study to propose a novel 3-D compact PHP module that is not only

feasible for real applications but also dramatically raises the applied heat flux density as compared to the existing studies.

2. Experimental Apparatus

The schematic of the experimental apparatus and test section is shown in Figure 4. The experimental setup comprises an evaporator section, an air-cooling system for the condenser, and PHP circuitry. A data acquisition system is also enclosed for analyzing the performance. The evaporator section is made of copper blocks (54 mm × 60 mm) where heaters are embedded within. The bakelite board is installed beneath the copper block in order to minimize the heat loss. For the air-cooling system for the condenser, the air flow rate is regulated and controlled via three fans (120 × 120 × 15 mm^3). Thermocouples are used to measure the junction and surface temperature of PHP. A total of six T-type thermocouples are placed underneath the test evaporators for measuring the average junction temperature, and each evaporator contains three thermocouples which are denoted as $T_{E1\sim3}$ and $T_{E2\sim3}$. In the meantime, some 12 thermocouples are installed at the inlet and outlet of the evaporator and condenser to record the temperature variations in the PHP circuitry. The locations of the thermocouples measurement in the circuitry is schematically shown in Figure 5 and are termed as $T_{ER,1\sim3}$ and $T_{EL,1\sim3}$, $T_{CL,1\sim3}$, and $T_{CR,1\sim3}$. Note that the subscripts ER and EL are the locations at the right side and left side of the corresponding evaporator tube section and CR and CL represent the location at the right side and left side of the condenser, respectively. The ambient temperature falls within 25~27 °C, and the airflow are driven by three fans (Thermaltake CL-F038-PL12RE-A, 120 mm × 120 mm × 25 mm).
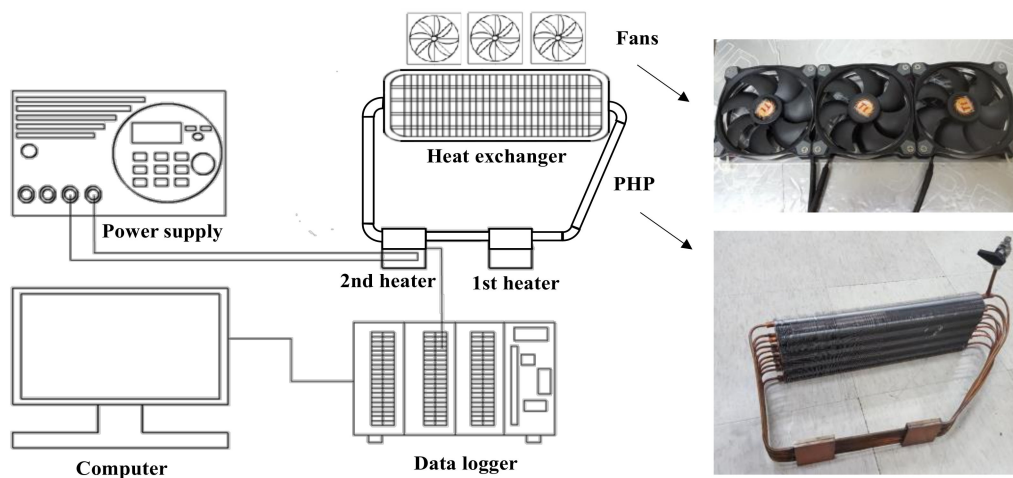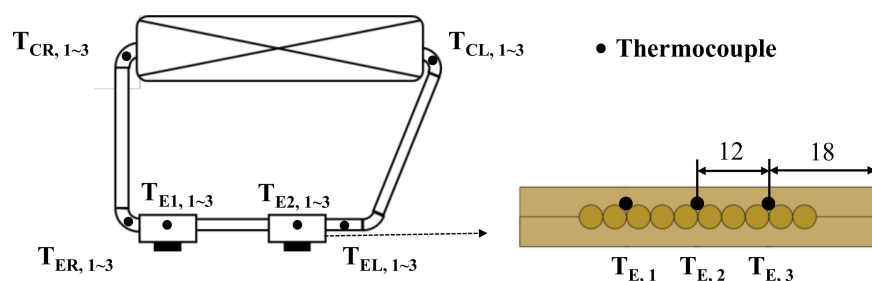

Figure 4. Experimental set up.

Figure 5. Schematic of the locations of the thermocouples (unit: mm).

Notice that there are 10 tubes used in the circuitry. To further elaborate the terminology, the corresponding tube numbering for condenser and evaporator can be seen in Figure 6a,b, respectively. The schematic of the PHP circuitry in terms of tube numbering is depicted in Figure 7a. These measured

temperature signals were individually recorded for further processing. During the isothermal test, the variation of these thermocouples was within 0.2 °C. In addition, all the thermocouples were pre-calibrated by a quartz thermometer having 0.04 °C precision. The accuracies of the calibrated thermocouples are of 0.1 °C. All the data signals are collected and converted by a data acquisition system (a hybrid recorder) as shown in Figure 4. The data acquisition system then transmitted the converted signals through an ethernet interface to the host computer for further operation.
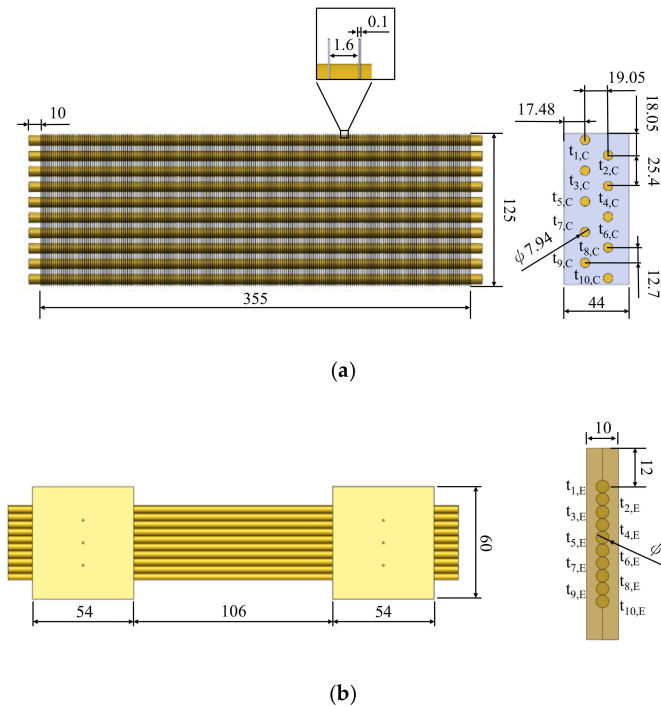

(a)

(b)

Figure 6. Detailed dimension of the (**a**) heat exchanger (**b**) cold plate (unit: mm).
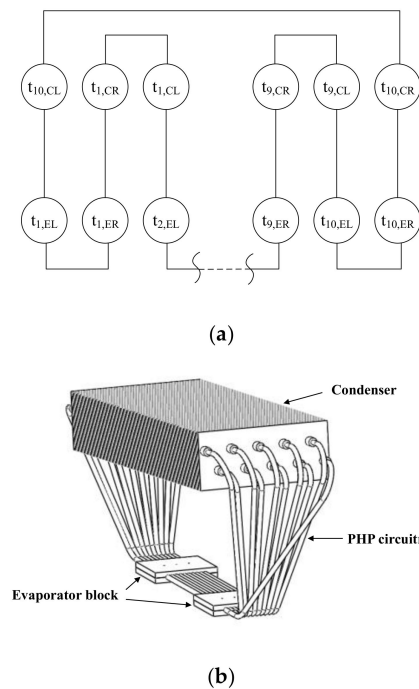

(a)

(b)

Figure 7. Schematic of (**a**) pipe connection (**b**) PHP thermal module.

The proposed PHP module consists of three parts, namely the (a) fin-and-tube heat exchangers; (b) evaporator bock for absorbing heat from the heat source; and (c) the pulsating heat pipe circuitry as shown in Figure 6b. Note that the tube part of the fin-and-tube heat exchanger acts as the condenser of the PHP. The fin-and-tube having a plain fin (aluminum alloy) configuration contains the following dimensions:

- Face area: 355 (W) $\times$ 125 (H) mm^2.
- Transverse tube and longitudinal tube pitch: 25.4 mm (P_t) and 19.05 mm (P_l), respectively.
- Fin pitch and fin thickness: 1.6 mm, and 0.1 mm, respectively.
- The number of tube rows: 2, with 5 rows in each tube row.
- Nominal outer tube diameter and inner diameter: 7.94 mm and 7.5 mm, respectively.

The outer diameter of the PHP circuitry is 4 mm with wall thickness being 0.3 mm. Notice that the condenser portion of the PHP circuitry makes use the existing fin-and-tube heat exchanger, thereby having an inner diameter of 7.5 mm in the condenser part. The tube is made of copper and contains a 10-turn design. The working fluid is methanol with an average filling ratio of 60% while the heating surface area is 60×54 mm^2 and is made of copper with backlite insulating around the heating element. The maximum heat input of this study is 1000 W provided by a power supply (GW INSTEK PSB-2400L2). The accuracies of the voltage and current are 0.2% and 0.3%, respectively. Uncertainties in the reported experimental values were estimated by the method suggested by Moffat [14]. The uncertainties are 1.58–2.24% for total thermal resistance.

3. Results and Discussion

Based on the analysis of the foregoing discussions, there are two main reasons associated with the low heat transfer performance of the PHP module. The first is associated with the high thermal resistance between evaporator and PHP ($R_{evap\text{-}BE}$), and the other is the loss of effective surface area due to the serpentine configuration. Take the references of Tseng et al. [9,10] and Sun et al. [11] as examples, the effective contact surface area in the evaporator is in the range of 9.12%–16.96%, suggesting that more than 80% of the evaporator surface area is ineffective as far as heat transfer is concerned. Yet the present novel thermal module design offers a 3-D configuration as seen in Figure 6b which can cover 66.67% of the contact surface area of the PHP alongside the evaporator. In addition, the fin-and-tube heat exchanger encompassing huge surface area is adopted to tackle the low thermal performance of air-cooling. Note that the fin-and-tube heat exchanger, as shown in Figure 5a, is commercially available with a very large surface area which can minimize the thermal resistance of the condenser. Figure 6 also depicts the current module design via integration of the 3-D PHP circuitry, evaporator, and condenser.

A typical temperature variation vs. elapsed time subject to change of heating power is shown in Figure 8. The startup characteristics are actually strongly related to the supplied power. As seen from Figure 8, by raising the supplied power from zero to 100 W, the PHP does not immediately respond to the supplied power. Hence, the relevant temperatures for all measurements reveal some massive rises, and it continues rising to 78 °C to launch the PHP. Once the PHP is initiated, the corresponding temperatures show a pronounced drop and temperatures start to fluctuate due to slug flow oscillation between the evaporator and condenser. It is clearly seen that there is barely any difference between the mean temperature at the entrance and exit of the condenser (T_{CR} and T_{CL}), implicating that slug flow oscillation between the condenser and evaporator plays the essential role of heat transport. The temperatures continue to rise with similar fluctuations when the supplied power is increased further. However, there is a detectable temperature difference at the entrance and exit of the condenser when the supplied power reaches 1 kW. The temperature difference across the condenser suggests that the main flow phenomenon changes from oscillating slug flow into circulating slug flow in a unilateral direction. This can be also made clear through the lower temperature fluctuation in the evaporator.
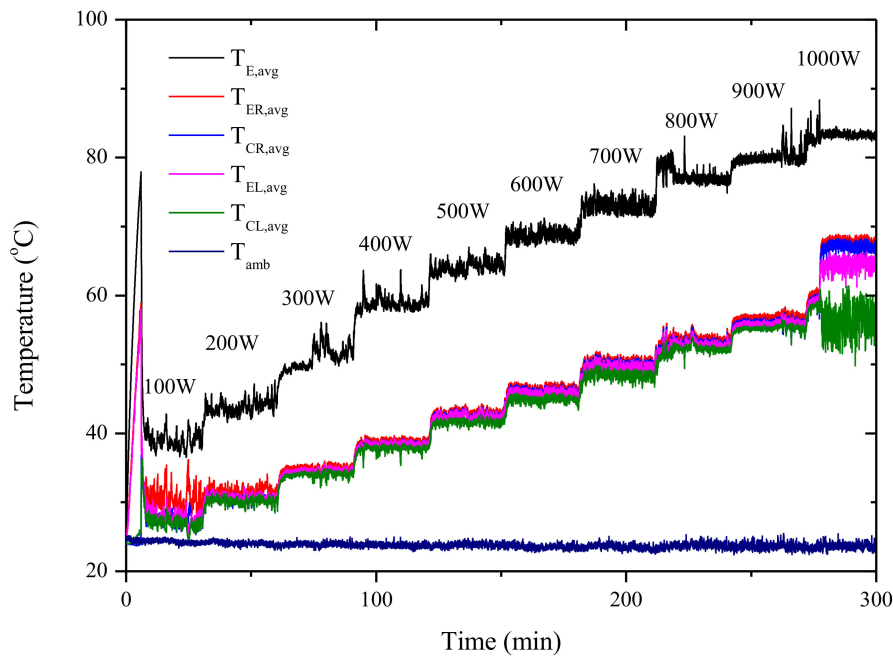
Figure 8. Temperature variation for the proposed PHP vs. elapsed time.

The corresponding thermal resistance vs. supplied power is shown in Figure 9. As seen in the figure, the thermal resistance varies from 0.148 K/W to 0.0595 K/W when the supplied power is raised from 100 to 1000 W. The thermal resistance shows a prominent decline with supplied power, indicating significant improvement caused by the oscillating slug. Correspondingly, the junction temperatures increases from 38.87 to 83.19 °C.
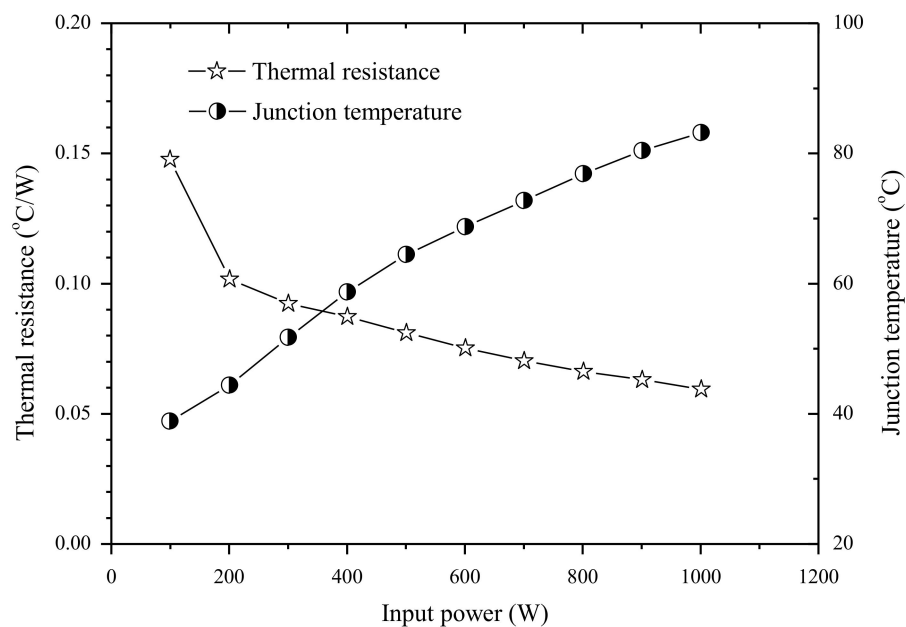

Figure 9. Thermal resistance and junction temperature vs. heating power of the PHP thermal module.

For further elaborations of the variations of thermal resistance in PHP thermal module, the total thermal resistance obtained from Equation (1) comprise thermal resistance of evaporator to PHP ($R_{E\text{-}EL}$), evaporator to condenser ($R_{EL\text{-}C}$), and condenser to ambient ($R_{CL\text{-}amb}$), respectively, as depicted in Equations (2)–(4).

$$R_{total} = \left(\bar{T}_E - T_{amb} \right) / Q_{in} \tag{1}$$

$$R_{E-EL} = \left(\bar{T}_E - T_{EL} \right) / Q_{in} \tag{2}$$

$$R_{EL-CL} = (T_{EL} - T_{CL}) / Q_{in} \tag{3}$$

$$R_{CL-amb} = (T_{CL} - T_{amb}) / Q_{in} \tag{4}$$

Note that T_E, T_{EL}, T_{CL}, and T_{amb} represent the average temperatures measured at the evaporator, EL, CL, sections and ambient as seen in Figure 5. The R_{E-EL}, R_{EL-CL}, R_{CL-amb} regarded to the thermal resistance of evaporator to PHP, evaporator to condenser section of PHP, and condenser to ambient. The corresponding fraction of thermal resistance ratio vs. supplied power is shown in Figure 10. As seen in the figure, the thermal resistance of the evaporator to the condenser section of the PHP (R_{EL-CL}/R_{total}) is only about 1% when the input power is over 300 W, indicating negligible influence of R_{EL-CL} on the overall performance. The thermal resistance ratio of the condenser to the ambient (R_{CL-amb}/R_{total}) is strongly related to the supplied power, and the ratio ranges form 21.6 % to 72.8% when the input power is raised from 100 W to 1000 W. The bottleneck of heat dissipation is the performance of condenser in high heating load applications. In this study, the utilization of a fin-and-tube heat exchanger with very large surface area can effectively minimize the thermal resistance of the condenser. The thermal resistance ratio of the evaporator to PHP (R_{E-EL}/R_{total}) is about 62.7–26.1%. In essence, the present novel thermal module design offers a 3-D configuration that can cover 66.67% of the contact surface area of the PHP alongside the evaporator.
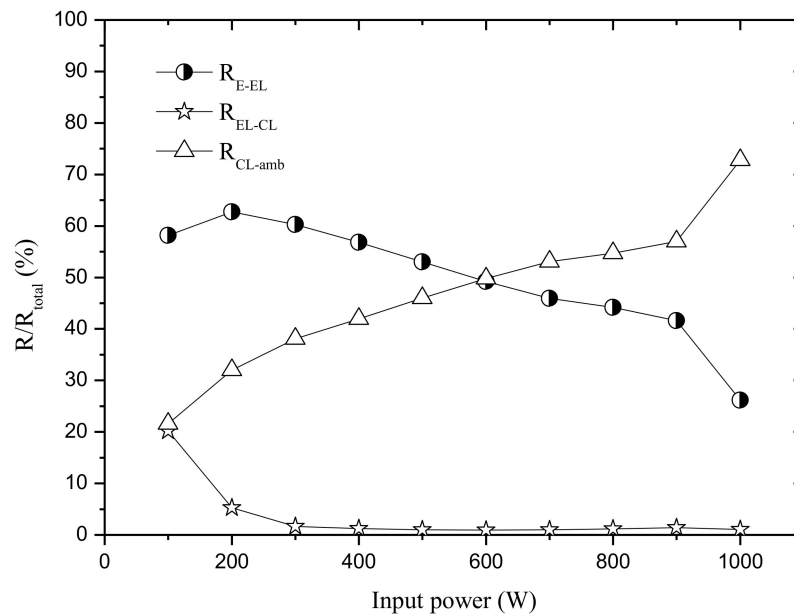

Figure 10. Thermal resistance ratio vs. input power of the PHP thermal module.

For further elaboration of the present test results, a comparison is made by thoroughly comparing the maximum heat flux and its relevant surface area with the existing literature [9,15–37] whose details are tabulated in Table 1. As shown in Figure 11, the present PHP module offers a maximum heat flux of 15.6 W/cm^2 that is significantly higher than in any existing literature. Yet the present design can handle a maximum power of 1000 W, which is also at least two times higher than in any of the exiting literature for a given surface area.

Table 1. References for comparison with this study and the corresponding major parameters.

References	Working Fluid	Filling Ratio	Surface Area (cm^2)	Maximum Heat Flux (W/cm^2)
Tseng et al. [9]	distilled water, methanol, HFE-7100	57.6–62.4%	161	0.87
Hathaway et al. [15]	water, acetone	62.5–62.7%	51.28	7.80
Mohammadi et al. [16]	ferrofluid, water	20–80%	70	6.86
Hu et al. [17]	self-rewetting	50%	18.4	6.52
Mohammadi et al. [18]	nanofluid, water	20–80%	196	0.71
Wilson et al. [19]	water, acetone	45–51%	60.45	4.96
Ji et al. [20]	nanofluid	50%	62	4.03
Riehl and Nadjara [21].	water, nanofluid	50%	70	0.71
Jahani et al. [22]	nanofluid	20–80%	16.2	1.73
Mohammadi et al. [23]	water, ferrofluid	40–70%	82	1.04
Yoon et al. [24]	water	51%	58.9	5.09
Karthikeyan et al. [25]	water	60%	132	3.79
Iwata et al. [26]	R134a		70	1.00
Ji et al. [27]	water, nanofluid	50%	62	3.23
Cui et al. [28]	water, methanol, acetone	0–100%	144	0.69
Liu et al. [29]	ethanol, methanol, water	0~100%	174	1.72
Lin et al. [30]	water	50%	18.4	7.61
Mameli et al. [31]	FC-72	50%	8.53	11.72
Zhao et al. [32]	nanofluid	50%	58.9	4.24
Patel and Mehta [33]	water, ethanol, methanol, acetone	50%	110	1.18
Kim et al. [34]	ethanol, water	50%	79.2	0.63
Ma et al. [35]	nanofluid	50%	180.6	1.86
Gamit et al. [36]	water	40–60%	136	0.37
Pastukhov and Maydanik [37]	R152a	40%	300	1.53
This study	methanol	60%	64.8	15.43
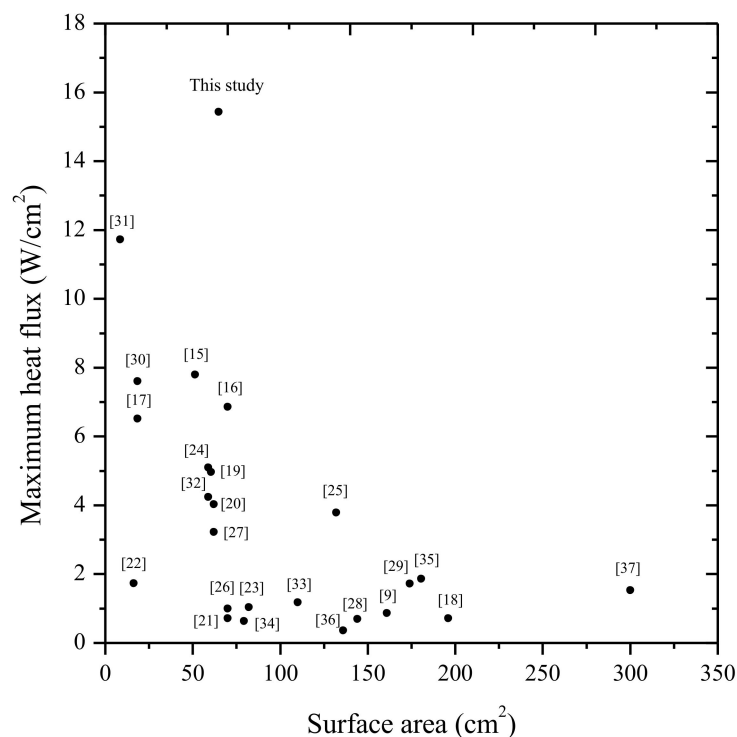
Figure 11. Comparison of the maximum heat flux vs. surface area of the present study against existing studies.

4. Conclusions

In this study, a novel 3-D structured PHP module is proposed to tailor high-flux cooling applications. The present novel thermal module design features are: (a) a 3-D configuration PHP circuitry; (b) an evaporator; and (c) a fin-and-tube condenser. The filling ratio of the thermal module is 60% with methanol as the working fluid. The proposed thermal module can handle a supplied heat input up to 1 kW with the thermal resistance varying from 0.148 K/W to 0.0595 K/W. Test results show that the overall thermal resistance continues to drop against the supplied power. The mechanism for heat removal is slug flow oscillation when the supplied heat is less than 800 W, and it changes to a unilateral direction slug flow when the supplied heat reaches 1 kW. There is a very small temperature variation between the inlet and exit of the condenser when the slug flow oscillation prevails. In the meantime, a detectable temperature difference across the condenser is observed when the supplied heat flux is 1 kW due to the presence of a unilateral direction slug flow pattern. The present PHP module offers a maximum heat flux of 15.6 W/cm^2 that is significantly higher than any existing literatures.

Nomenclature

A	area, (m^2)
cp	specific heat of water, (J/kg·K)
D	diameter, (m)
H	height, (m)
P	pressure, (Pa)
Pl	longitudinal pitch, (m)
P_t	transverse pitch, (m)
R	thermal resistance, (K/W)
T	temperature, (K)
W	width, (m)
Subscript	
amb	ambient
avg	average
BC	bend tube at condenser
BE	bend tube at evaporator
CL	left side of condenser
CR	right side of condenser
C	condenser
E	evaporator
EL	left side of evaporator
ER	right side of evaporator
SC	straight tube near condenser
SE	straight tube near evaporator

References

1. Chan, C.; Siqueiros, E.; Ling-Chin, J.; Royapoor, M.; Roskilly, A. Heat utilisation technologies: A critical review of heat pipes. *Renew. Sustain. Energy Rev.* **2015**, *50*, 615–627. [CrossRef]
2. Chen, X.; Ye, H.; Fan, X.; Ren, T.; Zhang, G. A review of small heat pipes for electronics. *Appl. Therm. Eng.* **2016**, *96*, 1–17. [CrossRef]
3. Faghri, A. Heat pipes: review, opportunities and challenges. *Front. Heat Pipes (FHP)* **2014**, *5*. [CrossRef]
4. Nazari, M.A.; Ahmadi, M.H.; Ghasempour, R.; Shafii, M.B.; Mahian, O.; Kalogirou, S.; Wongwises, S. A review on pulsating heat pipes: from solar to cryogenic applications. *Appl. Energy* **2018**, *222*, 475–484. [CrossRef]
5. Goshayeshi, H.; Goodarzi, M.; Dahari, M. Effect of magnetic field on the heat transfer rate of kerosene/Fe2O3 nanofluid in a copper oscillating heat pipe. *Exp. Therm. Fluid Sci.* **2015**, *68*, 663–668. [CrossRef]
6. Chien, K.H.; Lin, Y.T.; Chen, Y.R.; Yang, K.S.; Wang, C.C. A novel design of pulsating heat pipe with fewer turns applicable to all orientations. *Int. J. Heat Mass Transf.* **2012**, *55*, 5722–5728. [CrossRef]
7. Yang, K.-S.; Cheng, Y.-C.; Jeng, M.-S.; Chien, K.-H.; Shyu, J.-C. An Experimental Investigation of Micro Pulsating Heat Pipes. *Micromachines* **2014**, *5*, 385–395. [CrossRef]
8. Yang, K.-S.; Cheng, Y.-C.; Liu, M.-C.; Shyu, J.-C. Micro pulsating heat pipes with alternate microchannel widths. *Appl. Therm. Eng.* **2015**, *83*, 131–138. [CrossRef]
9. Tseng, C.-Y.; Yang, K.-S.; Chien, K.-H.; Jeng, M.-S.; Wang, C.-C. Investigation of the performance of pulsating heat pipe subject to uniform/alternating tube diameters. *Exp. Therm. Fluid Sci.* **2014**, *54*, 85–92. [CrossRef]
10. Tseng, C.-Y.; Yang, K.-S.; Chien, K.-H.; Wu, S.-K.; Wang, C.-C. A novel double pipe pulsating heat pipe design to tackle inverted heat source arrangement. *Appl. Therm. Eng.* **2016**, *106*, 697–701. [CrossRef]
11. Sun, C.-H.; Tseng, C.-Y.; Yang, K.-S.; Wu, S.-K.; Wang, C.-C. Investigation of the evacuation pressure on the performance of pulsating heat pipe. *Int. Commun. Heat Mass* **2017**, *85*, 23–28. [CrossRef]
12. Khandekar, S.; Dollinger, N.; Groll, M. Understanding operational regimes of closed loop pulsating heat pipes: an experimental study. *Appl. Therm. Eng.* **2003**, *23*, 707–719. [CrossRef]
13. Xu, D.; Li, L.; Liu, H. Experimental investigation on the thermal performance of helium based cryogenic pulsating heat pipe. *Exp. Therm. Fluid Sci.* **2016**, *70*, 61–68. [CrossRef]
14. Moffat, R.J. Describing the uncertainties in experimental results. *Exp. Therm. Fluid Sci.* **1988**, *1*, 3–17. [CrossRef]
15. Hathaway, A.; Wilson, C.; Ma, H. Experimental investigation of uneven-turn water and acetone oscillating heat pipes. *J. Thermophys. Heat Transf.* **2012**, *26*, 115–122. [CrossRef]
16. Mohammadi, M.; Taslimifar, M.; Saidi, M.H.; Shafii, M.B.; Afshin, H.; Hannani, S.K. Ferrofluidic open loop pulsating heat pipes: efficient candidates for thermal management of electronics. *Exp. Heat Transf.* **2014**, *27*, 296–312. [CrossRef]
17. Hu, Y.; Liu, T.; Li, X.; Wang, S. Heat transfer enhancement of micro oscillating heat pipes with self-rewetting fluid. *Int. J. Heat Mass Tranf.* **2014**, *70*, 496–503. [CrossRef]
18. Mohammadi, M.; Taslimifar, M.; Haghayegh, S.; Hannani, S.K.; Shafii, M.B.; Saidi, M.H.; Afshin, H. Open-loop pulsating heat pipes charged with magnetic nanofluids: powerful candidates for future electronic coolers. *Nanoscale Microscale Therm. Eng.* **2014**, *18*, 18–38. [CrossRef]
19. Wilson, C.; Borgmeyer, B.; Winholtz, R.; Ma, H.; Jacobson, D.; Hussey, D. Thermal and visual observation of water and acetone oscillating heat pipes. *J. Heat Transf.* **2011**, *133*, 061502. [CrossRef]
20. Ji, Y.; Ma, H.; Chen, H.-H. Volume fraction effect on heat transfer performance of an oscillating heat pipe. *J. Thermophys. Heat Transf.* **2012**, *27*, 111–115. [CrossRef]
21. Riehl, R.R.; dos Santos, N. Water-copper nanofluid application in an open loop pulsating heat pipe. *Appl. Therm. Eng.* **2012**, *42*, 6–10. [CrossRef]
22. Jahani, K.; Mohammadi, M.; Shafii, M.B.; Shiee, Z. Promising technology for electronic cooling: Nanofluidic micro pulsating heat pipes. *J. Electron. Packag.* **2013**, *135*, 021005. [CrossRef]
23. Mohammadi, M.; Mohammadi, M.; Shafii, M. Experimental investigation of a pulsating heat pipe using ferrofluid (magnetic nanofluid). *J. Heat Transf.* **2012**, *134*, 014504. [CrossRef]
24. Yoon, I.; Wilson, C.; Borgmeyer, B.; Winholtz, R.; Ma, H.; Jacobson, D.; Hussey, D. Neutron phase volumetry and temperature observations in an oscillating heat pipe. *Int. J. Therm. Sci.* **2012**, *60*, 52–60. [CrossRef]
25. Karthikeyan, V.; Khandekar, S.; Pillai, B.; Sharma, P.K. Infrared thermography of a pulsating heat pipe: Flow regimes and multiple steady states. *Appl. Therm. Eng.* **2014**, *62*, 470–480. [CrossRef]

26. Iwata, N.; Ogawa, H.; Miyazaki, Y. Temperature-controllable oscillating heat pipe. *J. Thermophys. Heat Transf.* **2011**, *25*, 386–392. [CrossRef]
27. Ji, Y.; Ma, H.; Su, F.; Wang, G. Particle size effect on heat transfer performance in an oscillating heat pipe. *Exp. Therm. Fluid Sci.* **2011**, *35*, 724–727. [CrossRef]
28. Cui, X.; Zhu, Y.; Li, Z.; Shun, S. Combination study of operation characteristics and heat transfer mechanism for pulsating heat pipe. *Appl. Therm. Eng.* **2014**, *65*, 394–402. [CrossRef]
29. Liu, X.; Chen, Y.; Shi, M. Dynamic performance analysis on start-up of closed-loop pulsating heat pipes (CLPHPs). *Int. J. Therm. Sci.* **2013**, *65*, 224–233. [CrossRef]
30. Lin, Z.; Wang, S.; Chen, J.; Huo, J.; Hu, Y.; Zhang, W. Experimental study on effective range of miniature oscillating heat pipes. *Appl. Therm. Eng.* **2011**, *31*, 880–886. [CrossRef]
31. Mameli, M.; Araneo, L.; Filippeschi, S.; Marelli, L.; Testa, R.; Marengo, M. Thermal response of a closed loop pulsating heat pipe under a varying gravity force. *Int. J. Therm. Sci.* **2014**, *80*, 11–22. [CrossRef]
32. Zhao, N.; Zhao, D.; Ma, H. Experimental investigation of magnetic field effect on the magnetic nanofluid oscillating heat pipe. *J. Therm. Sci. Eng. Appl.* **2013**, *5*, 011005. [CrossRef]
33. Patel, V.M.; Mehta, H.B. Influence of working fluids on startup mechanism and thermal performance of a closed loop pulsating heat pipe. *Appl. Therm. Eng.* **2017**, *110*, 1568–1577. [CrossRef]
34. Kim, B.; Li, L.; Kim, J.; Kim, D. A study on thermal performance of parallel connected pulsating heat pipe. *Appl. Therm. Eng.* **2017**, *126*, 1063–1068. [CrossRef]
35. Ma, H.; Wilson, C.; Yu, Q.; Park, K.; Choi, U.; Tirumala, M. An experimental investigation of heat transport capability in a nanofluid oscillating heat pipe. *J. Heat Transf.* **2006**, *128*, 1213–1216. [CrossRef]
36. Gamit, H.; More, V.; Mukund, B.; Mehta, H. Experimental investigations on pulsating heat pipe. *Energy Procedia* **2015**, *75*, 3186–3191. [CrossRef]
37. Pastukhov, V.; Maydanik, Y.F. Development of a pulsating heat pipe with a directional circulation of a working fluid. *Appl. Therm. Eng.* **2016**, *109*, 155–161. [CrossRef]